HyperSLICE: HyperBand optimised Spiral for Low-latency Interactive Cardiac Examination

Submitted to Journal of Magnetic Resonance Imaging (JMRI)

Dr. Olivier Jaubert¹, Dr. Javier Montalt-Tordera¹, Dr. Daniel Knight^{1,3}, Pr. Simon Arridge², Dr. Jennifer Steeden¹, Pr. Vivek Muthurangu¹

^{1.} UCL Centre for Cardiovascular Imaging, University College London, London. WC1N 1EH. United Kingdom

² Department of Computer Science, University College London, London. WC1E 6BT. United Kingdom

^{3.} Department of Cardiology, Royal Free London NHS Foundation Trust, London. NW3 2QG. United Kingdom.

Corresponding author:

Name Olivier Jaubert

Department Centre for Translational Cardiovascular Imaging

Institute University College London

Address 30 Guilford St, London WC1N 1EH

E-mail o.jaubert@ucl.ac.uk

Acknowledgments: N/A

Grant Support: This work was supported by UK Research and Innovation (MR/S032290/1), Heart Research UK (RG2661/17/20) and the British Heart Foundation (NH/18/1/33511, PG/17/6/32797).

<u>Running Title</u>: HyperSLICE for low-latency interactive cardiac examination.

Abstract

BACKGROUND: Interactive cardiac magnetic resonance imaging is used for fast scan planning and

MR guided interventions. However, the requirement for real-time acquisition and near real-time

visualization constrains the achievable spatio-temporal resolution.

PURPOSE: To improve interactive imaging resolution through optimization of undersampled spiral

sampling and leveraging of deep learning for low-latency reconstruction (deep artifact suppression).

STUDY TYPE: Retrospective/Prospective.

POPULATION: Deep artefact suppression training data consisted of 692 breath-held CINEs. The

developed interactive sequence was tested prospectively in 12 patients (10 for image evaluation, 2

during catheterization).

FIELDSTRENGTH/SEQUENCE: 1.5T, interactive variable density spiral balanced Steady State

Free Precession 2D sequence.

ASSESSMENT: In simulated data, NRMSE, pSNR and SSIM of radial, uniform spiral and optimized

spiral sampling were compared. In the prospective study, the optimized spiral interactive sequence

was compared to conventional Cartesian real-time, and breath-hold cine imaging in terms quantitative

and qualitative image metrics.

STATISTICAL TESTS: Friedman chi-squared tests with post-hoc Nemenyi test (p<0.05).

RESULTS: The NRMSE, pSNR and SSIM were all statistically significantly higher in simulations of

optimized spiral compared to radial and uniform spiral sampling, particularly after scan plan changes

(SSIM: 0.71 vs 0.45 and 0.43).

Prospectively, HyperSLICE proposed a higher spatial and temporal resolution than conventional

Cartesian real-time imaging. The pipeline was demonstrated in patients during catheter pull back

showing sufficiently fast reconstruction for interactive imaging.

DATA CONCLUSION: HyperSLICE enables higher spatial and temporal interactive imaging.

Optimizing the spiral sampling enabled better overall image quality and better handling of image

transitions compared to radial and uniform spiral trajectories.

Evidence Level: 1.

Technical Efficacy: Stage 1.

Introduction

Interactive cardiovascular magnetic resonance (MR) imaging combines real-time image acquisition with on-the-fly reconstruction and interactive scan-plane control. It is a vital requirement for MR guided cardiac interventions and is increasingly used for image planning, particularly in patients with complex anatomy. Unfortunately, conventional Cartesian interactive real-time imaging (1) is limited by relatively low spatial and temporal resolutions, which restrict the potential applications.

State-of-the-art approaches that combine k-space undersampling, efficient k-space filling and iterative reconstructions such as compressed sensing (CS) have enabled high spatial and temporal resolution real-time imaging (2–4). However, most of these algorithms are not applicable to interactive imaging due to their incompatibility with on-the-fly reconstruction.

An alternative approach is to use pretrained Machine Learning (ML) networks that can have short inference times when applied as a single pass post-processing step (deep artifact suppression) (3). We have previously demonstrated deep artifact suppression can be used to perform on-the-fly reconstruction of radially undersampled data, enabling high resolution interactive cardiac imaging (5). However, our previous approach suffered from suboptimal image quality during interactive scan-plane changes.

Therefore, we propose two modifications to remedy this problem: changing from radial to spiral sampling and changing the network architecture. Concerning the first point, spiral sampling is more efficient than radials but comes with many more degrees of freedom that must be optimized. Thus, in this study we attempt to 'find' the optimal variable density spiral trajectory, number of spiral arms and interleave ordering using a bandit-based approach - HyperBand (6). The HyperBand approach allows multiple sampling schemes to be tested during deep artefact suppression training. The sampling pattern combined with the accompanying artefact suppression network that produces the best image quality can then be used for subsequent prospective inference.

The second modification was to the network architecture used for deep artefact suppression. Our previous approach used recurrent convolutional neural networks (RCNN) that can process 2D images on-the-fly, but still benefits from temporal redundancies in the data. The main problems with RCNN's are divergence during training and inference, and slow transitions during scan plane changes (5). Consequently, we chose to use FastDVDnet (7) that has recently shown promising performance for real-time video denoising, especially in terms of inference times and the handling of image transitions.

The aims of this study were to: 1) jointly find the optimal spiral sampling pattern and train an optimum deep artefact suppression network for interactive imaging, 2) evaluate this optimized framework against radial and uniform spiral trajectories in simulations, with a focus on image transitions, 3) quantitively

and qualitatively compare images from the optimized framework, in a prospective cohort, to reference breath-hold Cartesian, real-time Cartesian, and CS reconstructions of the spiral data, 3) qualitatively demonstrate the feasibility of using this interactive acquisition and on-the-fly reconstruction during right heart catheter pull back.

Methods

This study was approved by the local research ethics committee (ref. 19/LO/1561), and written consent was obtained in prospective and retrospective cohorts.

Training Data

The training dataset used for the ML networks consisted of 692 ECG triggered breath-held Cartesian balanced steady-state free precession (bSSFP) CINE multi-coil raw data acquired on a 1.5T system (Aera, Siemens Healthineers, Erlangen, Germany). The dataset included seven different orientations (short axis -SAX-, 4 chamber -4CH-, 3 chamber -3CH-, 2 chamber -2CH-, right ventricular long axis -RVLA-, right ventricular outflow tract -RVOT-, and pulmonary artery -PA-) and was collected in a diverse adult patient population referred for routine cardiovascular MR.

The raw data was acquired with 2x undersampling (with nominal matrix size of 224x272 and 44 autocalibration lines) and reconstructed with GRAPPA to recover fully sampled reference Cartesian multi-coil k-spaces. From this data, both undersampled input and high-quality target output images were created. Target magnitude images were reconstructed through Fast Fourier Transformation (FFT) of the fully sampled Cartesian multi-coil k-space data and coil combination using root-sum-of-squares (RSS). The resultant ground truth images were scaled between 0 and 1 and the same scaling was applied to the multi-coil k-space data before undersampling. Undersampled input images (gridded images) were obtained by performing spiral undersampling of the rescaled multi-coil k-space data according to the investigated trajectories (as described below), followed by non-uniform FFT and RSS coil combination.

Network Architecture

FastDVDnet is a convolutional network architecture proposed for video denoising which conventionally takes five noisy frames as input and outputs the denoised central frame. This network architecture was empirically chosen for its high performance, fast runtimes, and its robustness to motion.

A modified FastDVDnet (Figure 1) was implemented using TensorFlow and Keras (8). Modifications included: 1) Reducing latency between acquisition and display by outputting the deep artefact suppressed last frame, 2) Empirically enhancing performance in our specific application with no global residual connection, no batch normalization, replacing the pixel-wise addition with a more classic channel-wise concatenation and replacing the loss by a structural similarity index (SSIM) based loss.

Our modified FastDVDnet network takes five consecutive frames of undersampled coil combined gridded magnitude data as inputs, and outputs the deep artifact suppressed fifth magnitude image (Figure 1A). The FastDVDnet network consists of four denoising blocks, all of which have the same architecture, shown in Figure 1B, where the three "Denoising Blocks 1" of the first layer share the same weights. The network is then applied in a sliding window fashion to output consecutive 2D frames (excluding first four frames of the series).

HyperBand Optimization

HyperBand is a bandit-based technique that makes minimal assumptions and aims at speeding up the evaluation of many hyperparameter configurations. In this study we hyperparameterized six variables that controlled the variable density spiral arm shape (9), and the number and order of spiral interleaves. Each spiral arm is defined by five parameters: a k-space inner radius (parameter 1) with a given sampling density (parameter 2), a k-space outer radius (parameter 3) beyond which is a given sampling density (parameter 4), and a transition type (parameter 5, e.g. linear, Hanning or quadratic) which controls the density transition between the inner and outer radiuses of k-space. Additionally, the ordering of the spiral arms (parameter 6) could either be tiny golden angle (47.3°) or linear (number of arms/360°).

We defined the range of allowable repetition times (TR: [2.88, 3.7] ms) and maximum time per frame (T_{acq} : 55ms). The number of interleaves was then calculated as 'floored' value: T_{acq} /TR. The explored range of parameterized values was restricted to relevant values and are indicated in Table 1.

The trajectory optimization process is depicted in Supporting Information Figure S1. In brief, randomly parametrized spiral trajectories are generated and used to create paired undersampled and ground truth images that are used to train the FastDVDnet network. By monitoring validation SSIM it was possible to allocate more resources and continue the training of the most promising trajectory and network combinations.

The maximum resource allocated to a given configuration (i.e. maximum number of epochs) was set to 150, and the ratio of discarded to kept configurations between each step of the HyperBand algorithm was set to 5. This led to the modified FastDVDnet architecture being trained for 217 different spiral trajectories over a total of 3404 epochs. The configuration which resulted in deep artifact suppressed images with the best validation SSIM was selected for subsequent studies.

A subset of the dataset (40%) was used for HyperBand optimization to reduce overall training times. The data was split 30/10% for train/validation during the HyperBand parameter optimization of the spiral. Once the trajectory was selected, the network was then retrained with the whole dataset with a 75/10/15% split for training/validation/testing. All training was performed using TensorFlow (8) on a Linux Workstation (with NVIDIA TITAN RTX 24GB).

Simulation Experiments to Compare Sampling

The optimal spiral trajectory and deep artifact networks (as chosen by the HyperBand algorithm), were compared to tiny golden radial sampling (10) (with matching temporal resolution i.e. 17 radial spokes per frame) and a uniform density spiral trajectory (with TR and ordering matching those of the optimal trajectory) in simulation. For these two trajectories, the same network architecture was trained using the same dataset and fitting procedure as for the final optimized spiral trajectory network. A test set of 2D+time images, comprising of 15% of the dataset (103 CINEs), were undersampled, gridded and deep artefact suppressed using the appropriate network for each of these three trajectories.

Reconstructed simulated real-time data from the test set were assessed in terms of Normalized Root Mean Squared Error (NRMSE), peak SNR (PSNR) and SSIM. Metrics were averaged over five consecutive frames of a cine in all subjects (total of 515 images). Additionally, SSIM mean and standard deviation over 103 cases was measured in twelve frames during which a sharp transition between two random CINEs from the test set occur (at frame six) to assess the performance during interactive scan plane changes.

Prospective Experiments

Prospective datasets were acquired in 10 patients undergoing routine cardiovascular MR. In each subject, three separate long axis (4 CH, 3CH and 2CH orientations) cine data were acquired with: 1) the optimized spiral trajectory – HyperSLICE – pixel size 1.7x1.7mm², temporal resolution 55ms, 2) an ECG triggered breath-held Cartesian reference sequence – nominal pixel size 1.5x1.5mm², temporal resolution 27.3ms (~10s breath-hold), and 3) a real-time Cartesian sequence – pixel size 2.5x2.5mm², temporal resolution 97ms. Full acquisition parameters in Supporting Information Table S1.

HyperSLICE interactive images were reconstructed in near real-time during scanning using Gadgetron (11) for low-latency communication with an external computer (Linux Workstation with NVIDIA GeForce RTX 3060 12GB, where reconstruction times were recorded). The optimized spiral raw data were also retrospectively reconstructed using a simple gridded reconstruction (the equivalent to the input to the network) and compressed sensing (CS) with Temporal Total Variation reconstruction (alternating method of multipliers, λ =5*10-5). The gridded and CS reconstructions were performed offline using TensorFlow-MRI (12). The Cartesian datasets used for comparison were reconstructed on the scanner platform using the scanner software reconstructions (GRAPPA) (16).

Image quality was assessed using quantitative and qualitative metrics. Edge Sharpness (ES) was evaluated quantitatively by measuring the maximum gradient of the normalized pixel intensities between left ventricular (LV) blood pool and LV myocardium at peak diastole using four line profiles drawn manually (13). The line profiles were filtered using a Savitzky-Golay filter (window width, 8 pixels; third-order polynomial) to remove contamination with noise pixels. Signal to Noise Ratio (SNR)

was estimated quantitively as the ratio between signal in the LV blood pool and empty lung region for all CINEs at peak diastole. Because the signal is estimated from magnitude images, a correction factor of 0.66 is applied to account for the non-Gaussian noise distribution (14).

Subjective image quality of all but the gridded images were assessed by two clinical experts (V.M., D.K) in terms of motion depiction, presence of artefacts and sharpness of the endocardial border according to a 5-point Likert scale (1 = non-diagnostic, 2 = poor, 3 = adequate, 4 = good, 5 = excellent image quality).

Additionally, two patients were scanned using HyperSLICE during routine catheter pull back that is usually performed without imaging towards the end of right heart catheterization (RHC). During the acquisition, the operator interactively moved the slice position to track the catheter for visualization of its position and movements. Gridded, CS and HyperSLICE images of the same acquisition were qualitatively compared.

Statistical Analysis

Friedman chi-squared tests were performed for repeated measures non-parametric distributions. When results were deemed significant (p<0.05), a post-hoc Nemenyi test was performed to test all pairwise correspondences and statistical significances (p<0.05). All statistical tests were performed in Python using scipy.

Results

HyperBand Optimization

HyperBand optimization took \sim 6 days during which 217 different spiral configurations were tested. An overview of the SSIM curves for tested configurations are depicted in Supporting Information Figure S1. The trajectories and gridded images for the trajectories with the five highest validation SSIM are shown in Figure 2 (corresponding trajectory parameters in Supporting Information Table S2). Compared to uniform density spiral sampling, the optimized trajectories are heavily sampled in the center of k-space with high undersampling factors in the outer portion of k-space. This results in spatial blurring and light aliasing rather than the heavy undersampling artefacts observed in radial and uniform spiral undersampled images. It should be noted that the best sampling pattern had linear rather than tiny golden angle ordering.

Simulation Results

NRMSE, PSNR and SSIM mean and standard deviation over the test dataset (n=103) are provided in Table 2. NRMSE, PSNR and SSIM were all statistically significantly higher for the optimized trajectory

compared to radial and uniform density spiral trajectories. Interestingly results also show that the radial trajectory performed statistically significantly better than the uniform spiral.

Figure 3.A shows image quality obtained during scan plane changes with Figure 3.B showing the corresponding drop and recovery of SSIM through time. The drop in image quality during transitions was minimal for the optimized spiral trajectory compared to radial and uniform spiral sampling with an average SSIM of 0.71 immediately after transition (vs 0.45 and 0.43 for radial and uniform spiral respectively).

Prospective Results

Representative X-Y images and X-T profiles from prospectively acquired data in two orientations (3CH and 4CH) for reference, Cartesian real-time, spiral gridded, spiral CS and HyperSlice methods are presented in Figure 4. Subjective scoring (Table 3), HyperSLICE showed significantly (p<0.05) better image sharpness and motion depiction compared to real-time Cartesian interactive, but slightly more image artefacts. HyperSLICE also significantly (p<0.05) outperformed CS reconstruction according to all subjective metrics.

Quantitative SNR and Edge sharpness values are provided in Table 3, with HyperSLICE having similar SNR to real-time Cartesian interactive images, but significantly greater edge sharpness.

Compared to the acquisition time of 55ms, the gridded reconstruction took on average 33 ms, deep artifact suppression 19 ms and other processes 5ms (including scaling and formatting). However, as the pipeline can perform gridding and deep artifact suppression of separate images in parallel, the proposed framework has a theoretical maximum output of one frame every 33ms.

Finally, HyperSLICE was demonstrated interactively during catheter pull back in Supporting Information Video S1 and S2. In Supporting Information Video S1, both the interactive interface and operator movements are displayed, demonstrating true interactive imaging during catheter tracking. Supporting Information Video S2 shows only the HyperSLICE images acquired in a second patient for better visualization. Figure 5 shows a comparison of the same real-time data acquired during catheter tracking, reconstructed using gridding, CS and HyperSLICE. The CS reconstruction uses temporal total variation which seems to blur out the catheter motion compared to the gridded and HyperSLICE reconstructions. Compared to the gridded images, HyperSLICE improved image quality by cleaning up remaining undersampling artefacts and recovering image sharpness.

Discussion

In this study, we designed a variable density spiral imaging framework for interactive imaging. The main findings of this study were: 1) HyperBand selected an optimal spiral sampling pattern that was

much more heavily sampled in the middle of k-space than the outer portions, ii) In simulations the optimal spiral sampling pattern (and associated deep artefact suppression) provided better image quality than either uniform density spiral or radial sampling, iii) In-vivo the optimal sampling pattern (and associated deep artefact suppression) provided higher spatio-temporal resolution compared to conventional Cartesian interactive imaging and superior image quality compared to CS reconstruction of the spiral raw data, and iv) The optimized framework provided high quality interactive imaging during MR guided cardiac catheterization.

HyperBand Optimization

Our previous study using radial sampling and deep artefact suppression demonstrated that high resolution interactive real-time imaging was possible, however imaging could still be improved. In this study we decided to move to more efficient spiral sampling to further improve image quality, particularly during scan plane transitions. An important aspect of imaging is optimization of the sampling pattern and several studies have used ML to learn the optimal sampling through differentiable parameterization of trajectories (15–17). However, with differentiable parametrizations it would have not been possible to search for variable numbers of spiral arms, different orderings, and different density transitions. Therefore, we used a bandit-based approach that enables more freedom on the choice of trajectories and is more appropriate for our non-differentiable optimization problem. Compared to uniform density spiral sampling, the top five trajectories were much more heavily sampled in the center of k-space. This resulted in spatially blurred and lightly aliased images rather than heavily aliased images. This suggests that the superior reconstruction for this application is closer to deep super resolution rather than deep artefact suppression. It should be noted that all the reconstructed images from the five top sampling patterns were within 0.01 SSIM points, even though the input gridded images have some significant differences. This demonstrates that the HyperBand algorithm can search widely in parameter space to provide a variety of good candidates.

Our HyperBand framework was optimized for spiral bSSFP imaging, but optimization could easily be done for other spiral sequences. For example, spiral sampling could be optimized for low flip angle GRE sequence, which are desirable for intervention due to low heating of metallic guidewires. In addition, the low level of assumptions means the same method could easily be optimized for other types of trajectories (e.g. variable density radial, or rosette) with no requirements for developing new parametrizations that are differentiable with respect to the loss.

Simulations Experiments

In simulations, the optimized spiral provided superior image quality compared to radial and uniform spiral sampling. This was particularly visible during abrupt scan plane changes, with both uniform spiral and radial sampling demonstrating poor image quality for several frames after the transition. We believe that this is because the optimized spiral gridded images contain significantly less artefact

than both the uniform spiral and radial gridded images. This means that the optimized network does not need to rely as heavily on previous frames (compared to radial or uniform spiral networks) leading to much better handling of transitions.

Interestingly, both radial and uniform spiral sampling demonstrated similarly low image quality compared to HyperSLICE, including during transitions in synthetic data. This has two important implications: i) Changing to a spiral trajectory alone is not sufficient for good image quality and some form of trajectory optimization is necessary and ii) Changing the network architecture alone did not prevent sub-optimal image quality during transitions. Although, replacing the RNN may not have been vital for improved image quality during transitions, the FastDVD network did provide much more stable training, with no divergence over time at inference. This is vital for robust use during clinical imaging and the FastDVD network provides good quality images with low enough inference times. Nevertheless, more recent video denoising architectures and improved realistic simulations of the input images could potentially provide better image reconstruction quality (18).

Prospective Experiments

In the in-vivo experiments, we demonstrated that HyperSLICE provided sharper and more motion accurate images than conventional Cartesian interactive imaging, due to the significantly higher spatio-temporal resolution. Improved resolution will be vital for greater use of interactive imaging in interventional MRI, as well as for direct cardiac evaluation as opposed to purely planning. The ML reconstruction performed better than CS, while additionally enabling interactive imaging. However, it should be noted that spiral acquired images did have more artefacts than conventional Cartesian images. This is unsurprising as the spiral acquisition is more highly accelerated. Furthermore, spiral sampling is more susceptible to trajectory errors which could lead to suboptimal reconstructed images. Including realistic sources of errors such as noise, off-resonance and gradient imperfections could lead to better results for both the trajectory selection, network training and final reconstructed image quality.

Study Limitations

Our framework was not used to perform actual catheter guidance as this was a proof-of-concept study. Further work is required to assess the specific improvements in clinical workflow and/or clinical relevance of higher spatial and temporal resolutions for interactive imaging applications.

Further optimization of image quality could be obtained by leveraging multi-coil raw data however including data consistency and coil sensitivity estimation is highly challenging due to the time constraints of this application.

The inference pipeline currently relies on GPU acceleration and an additional external computer to provide images with the necessary framerate which is not always available in the clinical setting.

Realistically, an optimized CPU implementation running directly on the scanner platform would be required for widespread use.

Conclusion

After optimization, a variable density spiral interactive acquisition and reconstruction framework, HyperSLICE, showed promising performance in terms of both image quality and reconstruction times and was successfully demonstrated during interactive cardiac MR-guided intervention enabling tracking during catheter pull back with higher spatial and temporal resolutions than conventional interactive imaging.

Figures

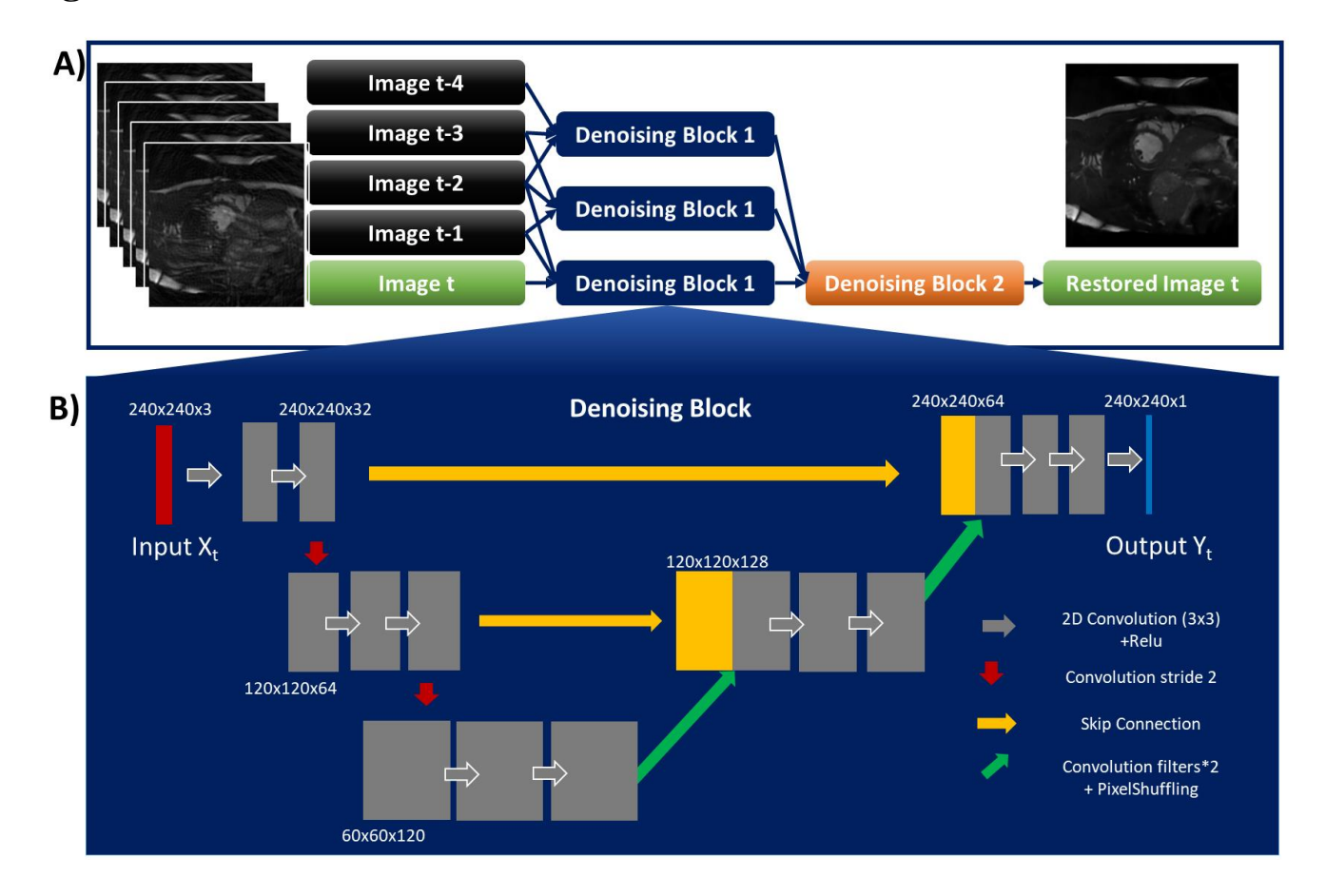


Figure 1. A) FastDVDNet modified architecture. Five consecutive undersampled magnitude frames are mapped to the fifth (i.e. latest) ground truth magnitude image for low-latency imaging. All denoising blocks share the same architecture with three input frames and one output frame. The three "Denoising Block 1" in the first layer share the same weights. **B)** The denoising block architecture. Main differences

to the original FastDVDnet denoising block include no global residual layer, no batch normalisation layer and concatenation after upsampling.

Spiral Parameters	Radius delimiting inner k- space	Inner acceleration rate	Radius delimiting outer k- space	Relative acceleration outer/inner	Transition	Ordering	TR (ms)	Temporal resolution (ms)	Inter- leaves	Accel. Rate
Range investigated	[0.1:0.3]	[12:24]	[inner:1- inner]	[0.01:0.35]	[linear, Hanning, quadratic]	[linear, tiny golden angle]	[2.88, 3.7]	<55	/	/
Optimized	0.15	16	0.56	0.07	Hanning	Linear	3.67	55	15	Variable [1.1,15.0]
Uniform	1	92	1	1	N/A	Linear	3.67	55	15	6.1

Table 1. Range of values tested in HyperBand optimization and resulting optimised spiral imaging parameters as well as matching uniform spiral parameters.

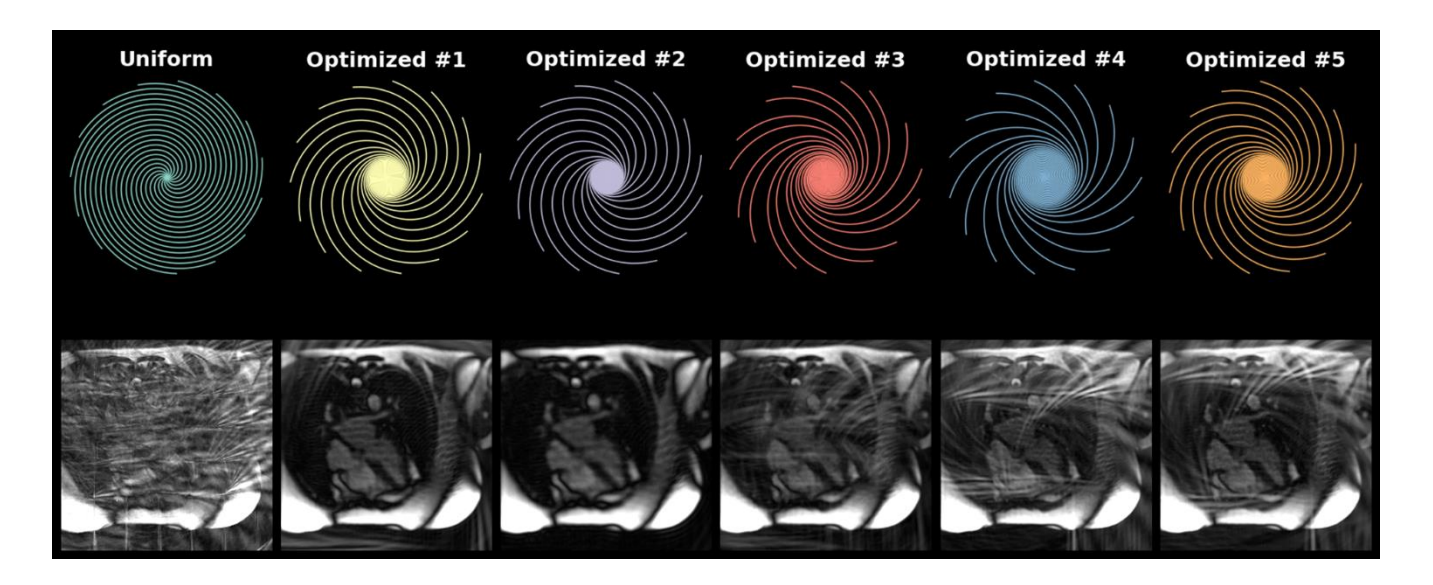


Figure 2. Uniform and top five variable density spiral trajectories obtained from the HyperBand optimization and corresponding Gridded images.

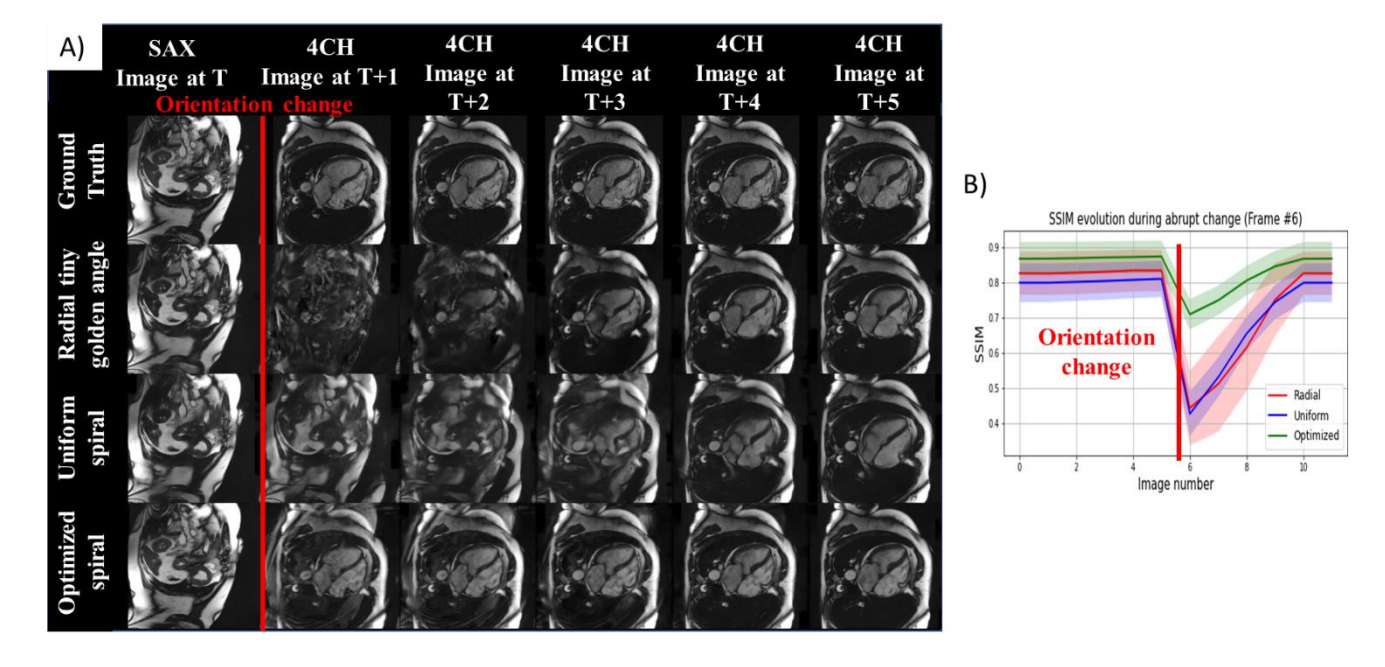


Figure 3. A) Image quality in simulation for six consecutive frames during abrupt scan-plane change from short axis (SAX) to four chambers (4CH). From top to bottom: ground truth and restored radial, uniform spiral and optimized spiral images. Optimized spiral results show better image quality and handling of transitions. **B)** Mean (± standard deviation) of SSIM through time during abrupt orientation change from radial, Uniform and Optimized Spiral Trajectories computed over 103 test cases.

Test results (n=103)	NRMSE	PSNR	SSIM
Radial	0.148 ±0.033	30.67 ±2.76	0.828 ±0.061
Uniform	0.171 ±0.028	29.33 ± 2.43	0.802 ± 0.054
Optimized	0.127 ± 0.026	31.99 ± 2.66	0.869 ± 0.047

Table 2. Mean and standard deviation of NRMSE, PSNR and SSIM computed over the test set images without scan plan change (103 slices x5 consecutive frames) for Radial, Uniform and Optimized Spiral reconstructed images.

^{*}All values are statistically significantly different from each other.

Prospective Experiment	SNR	Edge Sharpness (mm ⁻¹)	Subjective Image Sharpness	Subjective Artefacts	Subjective Motion
Reference Breath-hold	28.8 ±11.6	0.19 ±0.03	4.20 ±0.7	3.83 ±1.0	4.18 ±0.8
Real time Cartesian	38.3 ±11.7 [†]	0.18 ± 0.02	2.50 ± 0.6 [†]	3.78 ±0.5	$2.28 \pm\! 0.7^{\ \dagger}$
Spiral gridded	21.8 ±11.3 *	0.16 ± 0.03 †,+	N/A	N/A	N/A
Spiral CS	$26.0\ \pm 10.3\ ^*$	0.19 ± 0.04	$3.10~\pm0.9~^{\dagger,*}$	$2.15\ \pm0.5\ ^{\dagger,*}$	$3.05~\pm0.8~^{\dagger,*}$
HyperSLICE	46.8 ±30.4 ^{†,+}	0.21 ±0.04 *	3.67 ±0.5 *,+	3.18 ±0.6 †,*,+	3.77 ±0.4 *,+

Table 3. In-Vivo Results: Quantitative SNR, quantitative edge sharpness, subjective image sharpness, subjective artefact and subjective motion scores (1- Worst, 5-Best) mean values and standard deviation computed over the prospective images (10 subjects) for reference breath-hold, Cartesian real-time, spiral CS and HyperSLICE reconstructed images. Additionally includes spiral Gridded SNR and Edge sharpness.

Values with '†', '*' and '+' are statistically significantly different to reference breath-hold, real-time Cartesian and spiral CS values respectively (post-hoc Nemenyi test, p<0.05).

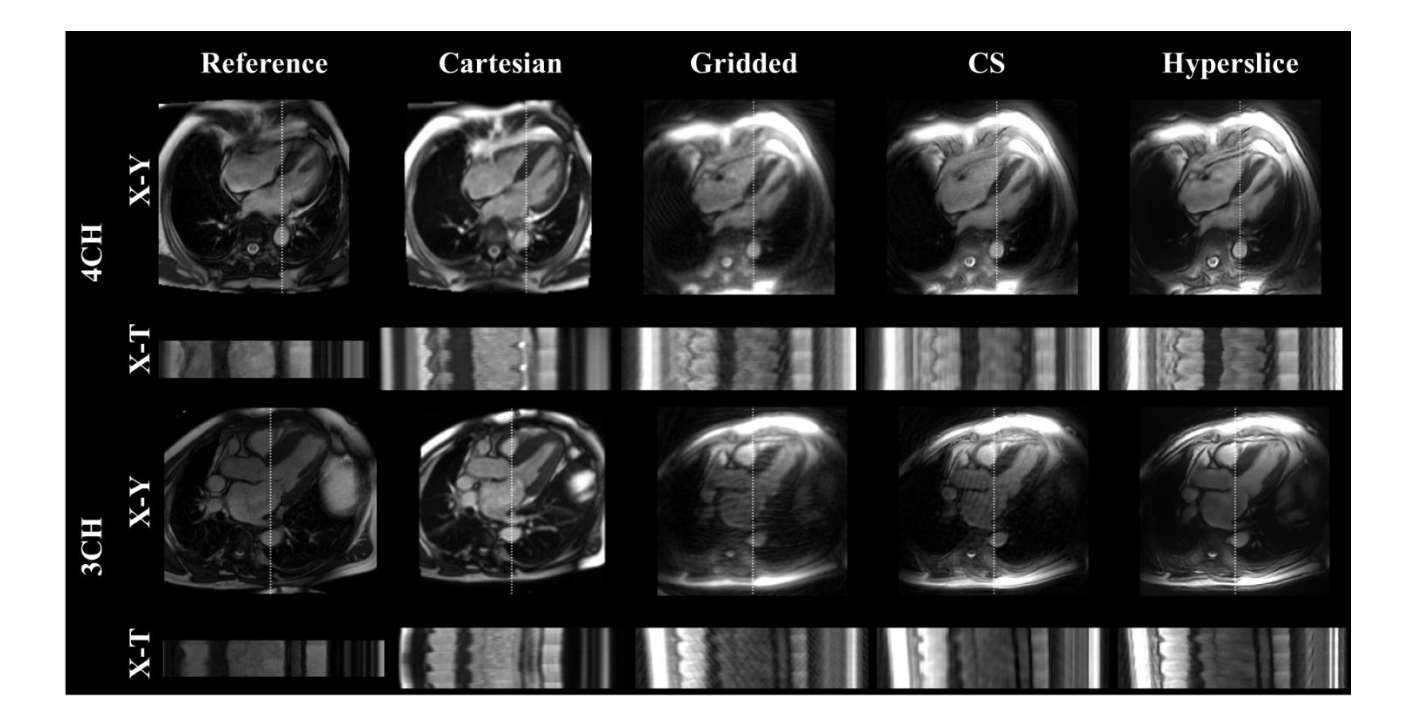


Figure 4. Qualitative In-Vivo Results: X-Y and X-T (white dotted line) views in the 4-chamber (Top) and 3-chamber (Bottom) orientations seen with reference breath-hold, Cartesian real-time, gridded, compress sensing (CS) and proposed HyperSLICE methods.

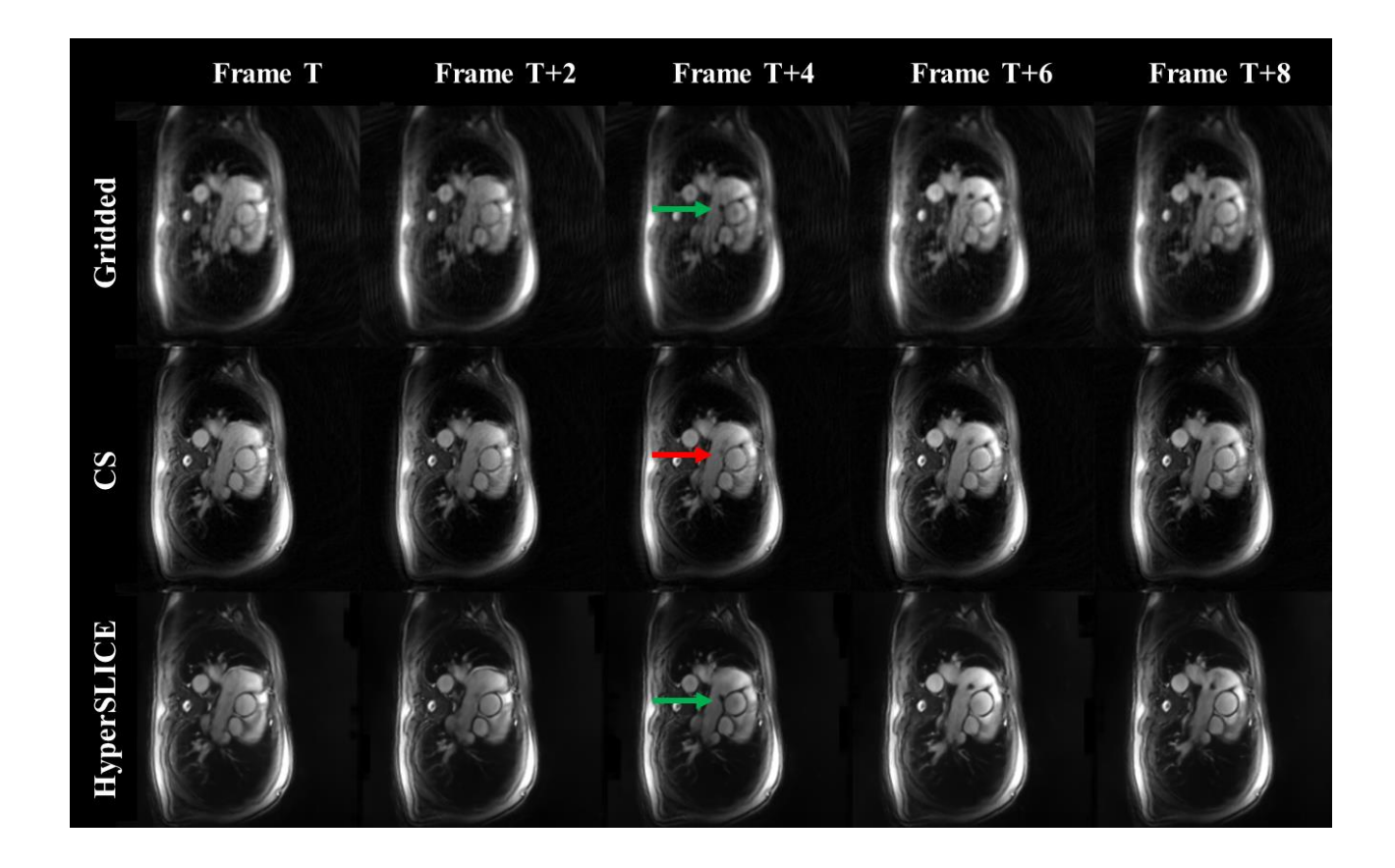


Figure 5. Prospective Catheter Images. Gridded, CS and HyperSLICE images of a sequence of images (every other frame shown). The catheter is indicated by the arrows in the central frames. The CS reconstruction with temporal total variation seems to blur out the catheter motion (red arrow) compared to the gridded and HyperSLICE reconstructions. HyperSlice demonstrates sharper edges and less artefacts than gridded images.

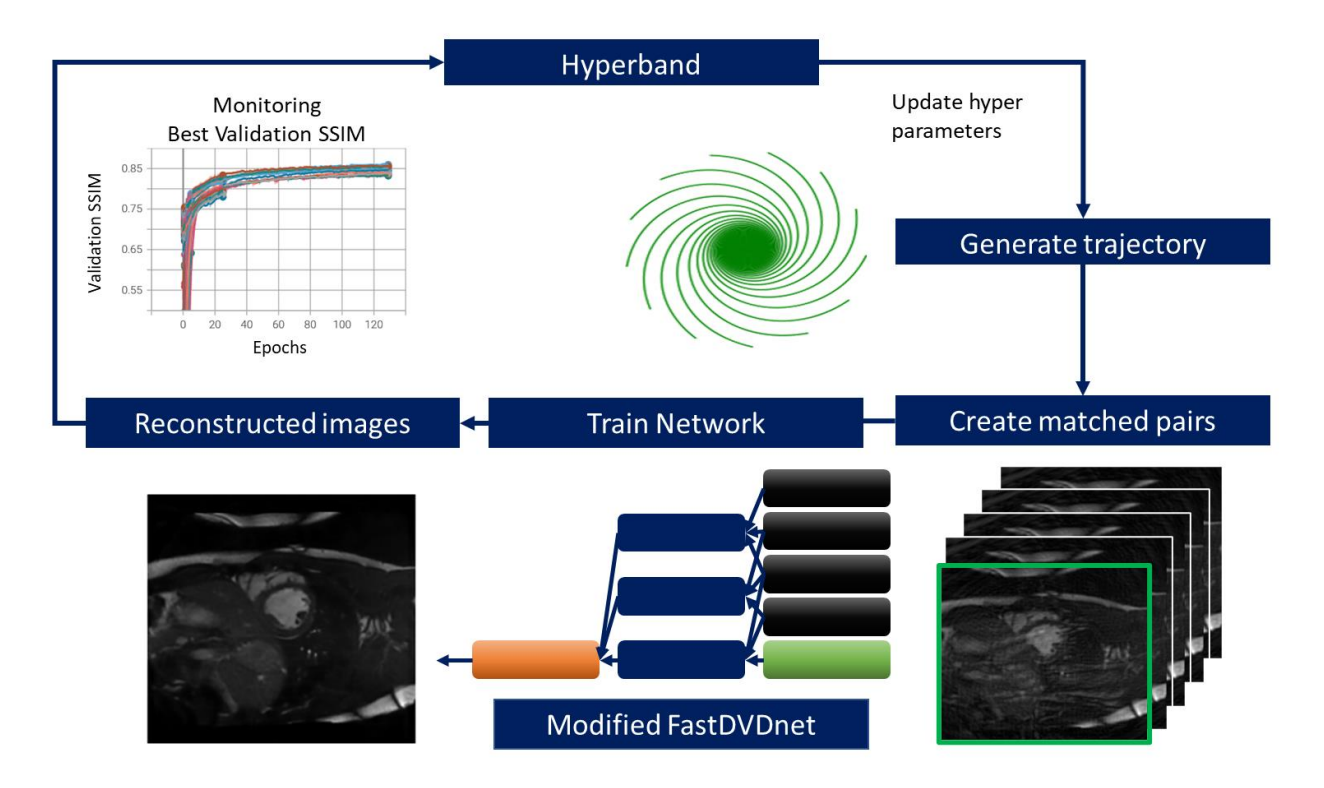
Supporting Figures

Acquisition Parameters	Туре	Spatial resolution (mm²)	Temporal Resolution (ms)	TE/TR (ms)	Flip Angle	Acceleration	Nominal FOV (mm²)
Reference Cartesian	Breath-hold	1.5x1.5	27.3	1.27/3.0	50	2	370x370
Real time Cartesian	Real time	2.5x2.5	97	0.98/2.4	50	2	320x320
Optimized Spiral	Real time	1.7x1.7	55	0.9/3.67	70	Variable density R=[1.1-15.0]	400x400

Supporting Information Table S1. Nominal acquisition parameters for reference Cartesian breathhold, real-time Cartesian and optimized spiral trajectories acquired prospectively in patients.

Spiral Parameters	End of inner k-space	Inner acceleration rate	Start of outer k-space	Relative acceleration outer/inner	Transition	Ordering	Validation SSIM
Range investigated	[0.1:0.3]	[12:24]	[inner:1-inner]	[0.01:0.35]	[linear, Hanning, quadratic]	[linear, tiny golden angle]	N/A
Optimized #1	0.15	16	0.60	0.07	hanning	linear	0.858
Optimized #2	0.16	12	0.40	0.05	linear	linear	0.856
Optimized #3	0.11	16	0.96	0.05	hanning	tiny	0.856
Optimized #4	0.24	24	0.95	0.06	hanning	linear	0.855
Optimized #5	0.22	21	0.68	0.09	linear	linear	0.851

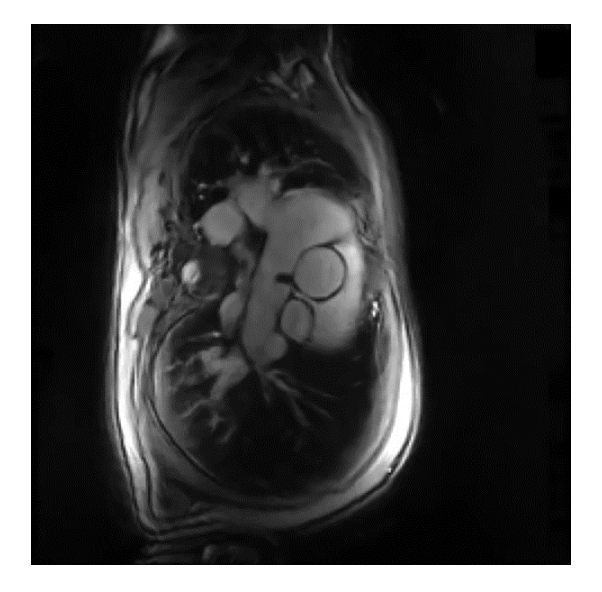
Supporting Information Table S2. The top five variable density spiral trajectories obtained from the HyperBand optimization.



Supporting Information Figure S1. Trajectory optimization through HyperBand: Hyperparameters to generate spiral trajectories are updated depending on the resulting SSIM scores obtained from deep artifact suppressed images. The trajectory shown in green corresponds to the resulting optimized trajectory (parameters in Table 1).



Supporting Information Video S1. Interactive imaging as performed on the scanner during catheter pull-back. The interface allows the user to move the scan plane and images update with minimal latency enabling immediate feedback on the location of the catheter.



Supporting Information Video S2. Interactive imaging during catheter pull-back in a second patient with suspected pulmonary hypertension.

References

- 1. Kerr AB, Pauly JM, Hu BS, et al. Real-time interactive MRI on a conventional scanner. Magn Reson Med 1997;38:355–367 doi: 10.1002/mrm.1910380303.
- 2. Feng L, Srichai MB, Lim RP, et al. Highly accelerated real-time cardiac cine MRI using k–t SPARSE-SENSE. Magn Reson Med 2013;70:64–74 doi: 10.1002/MRM.24440.
- 3. Hauptmann A, Arridge S, Lucka F, Muthurangu V, Steeden JA. Real-time cardiovascular MR with spatio-temporal artifact suppression using deep learning–proof of concept in congenital heart disease. Magn Reson Med 2019;81:1143–1156 doi: 10.1002/mrm.27480.
- 4. Lustig M, Donoho D, Pauly JM. Sparse MRI: The application of compressed sensing for rapid MR imaging. Magn Reson Med 2007;58:1182–1195 doi: 10.1002/mrm.21391.
- 5. Jaubert O, Montalt-Tordera J, Knight D, et al. Real-time deep artifact suppression using recurrent U-Nets for low-latency cardiac MRI. Magn Reson Med 2021;86:1904–1916 doi: 10.1002/MRM.28834.
- 6. Li L, Jamieson K, DeSalvo G, Rostamizadeh A, Talwalkar A. Hyperband: A Novel Bandit-Based Approach to Hyperparameter Optimization. Journal of Machine Learning Research 2016;18:1–52.
- 7. Tassano M, France G, Delon J, Veit T. FastDVDnet: Towards Real-Time Deep Video Denoising Without Flow Estimation. 2020:1354–1363.
- 8. Abadi M, Barham P, Chen J, et al. TensorFlow: A System for Large-Scale Machine Learning TensorFlow: A system for large-scale machine learning. Proceedings of the 12th USENIX Symposium on Operating Systems Design and Implementation 2016:265–283.
- 9. Pipe JG, Zwart NR. Spiral trajectory design: A flexible numerical algorithm and base analytical equations. Magn Reson Med 2014;71:278–285 doi: 10.1002/MRM.24675.
- 10. Winkelmann S, Schaeffter T, Koehler T, Eggers H, Doessel O. An Optimal Radial Profile Order Based on the Golden Ratio for Time-Resolved MRI. IEEE Trans Med Imaging 2007;26:68–76 doi: 10.1109/TMI.2006.885337.
- 11. Hansen MS, Sørensen TS. Gadgetron: An open source framework for medical image reconstruction. Magn Reson Med 2013;69:1768–1776 doi: 10.1002/mrm.24389.
- 12. Montalt Tordera J. TensorFlow MRI. 2022 doi: 10.5281/ZENODO.7120930.
- 13. Steeden JA, Atkinson D, Hansen MS, Taylor AM, Muthurangu V. Rapid flow assessment of congenital heart disease with high-spatiotemporal- resolution gated spiral phase-contrast MR imaging. Radiology 2011;260:79–87 doi: 10.1148/radiol.11101844.

- 14. McGibney G, Smith MR. An unbiased signal-to-noise ratio measure for magnetic resonance images. Med Phys 1993;20:1077–1078 doi: 10.1118/1.597004.
- 15. Aggarwal HK, Jacob M. J-MoDL: Joint Model-Based Deep Learning for Optimized Sampling and Reconstruction. 2019 doi: 10.1109/JSTSP.2020.3004094.
- 16. Wang G, Luo T, Nielsen JF, Noll DC, Fessler JA. B-Spline Parameterized Joint Optimization of Reconstruction and K-Space Trajectories (BJORK) for Accelerated 2D MRI. IEEE Trans Med Imaging 2022;41:2318–2330 doi: 10.1109/TMI.2022.3161875.
- 17. Zhang J, Zhang H, Wang A, et al. Extending LOUPE for K-space Under-sampling Pattern Optimization in Multi-coil MRI. 2020.
- 18. Cao J, Wang Q, Liang J, Zhang Y, Zhang K, van Gool L. Practical Real Video Denoising with Realistic Degradation Model. 2022 doi: 10.48550/arxiv.2208.11803.